Journal of Sound and Vibration (2000) **230**(5), 1103–1117
doi:10.1006/jsvi.1999.2671, available online at http://www.idealibrary.com on IDEAL®

EXPERIMENTAL INVESTIGATION OF DYNAMIC PROPERTIES OF AN ACTIVE JOURNAL BEARING

L. SUN AND J. M. KRODKIEWSKI

Department of Mechanical and Manufacturing Engineering, University of Melbourne, Parkville, Victoria 3052, *Australia*

(*Received* 4 *May* 1999, *and in final form* 10 *September* 1999)

A flexible sleeve can be considered as a new feature of the proposed active journal bearing. Variation of the oil pressure in the chamber located under the sleeve causes deformation of the sleeve and consequently changes the geometry of the oil film as well as the pressure distribution of the oil film. Hence, the dynamic characteristics of the bearing can be varied without stopping the operation of the rotor. Therefore, by changing the chamber pressure based on either pre-calculation or on-line processing, the dynamic response of the rotor could be controlled. This paper offers a detailed description of a laboratory installation furnished with the active bearing and the conducted experimental investigation. This experimental investigation allowed the developed mathematical models of the laboratory installation to be verified. Results of the numerical analysis of the dynamic response (stability of equilibrium position and forced response due to the residual imbalance) of the laboratory installation by means of both the linear and the non-linear mathematical model are presented. This analysis was carried out in both the configuration parameters domain and the angular speed domain. These analytical predictions are compared with results of the experimental investigation. Numerical calculations based on the mathematical model have shown good agreement with experimental results both qualitatively and quantitatively. Numerical calculations and the experiments indicate that the stability of the rotor-bearing system is sensitive to the chamber pressure of the active journal bearing. By applying an appropriate constant chamber pressure, the system stability can always be improved.

1. INTRODUCTION

In order to develop high performance rotating machinery, growing attention has been paid to active vibration control to improve the dynamic properties of the system by employing active devices. These active devices include magnetic bearings [1], piezoelectric bearing pushers [2], hydraulic actuator journal bearings [3], variable impedance bearings [4], deformable bushes [5] and active journal bearings with a flexible sleeve [6–8].

The mathematical model presented in reference [6] can be used to predict dynamic behaviours of multi-bearing rotor systems incorporating the presented active journal bearing with flexible sleeves. The linearized model is especially

0022-460X/00/101103 + 15 $35.00/0

suitable for an overall investigation of the system characteristics over a wide range of system configuration parameters and the rotating speed in which numerous combinations of configuration parameters need to be analyzed. Numerical simulations based on the non-linear model provide not only a measure to verify the validity of results from the linearized model, but also some important information about the system. The non-linear model provides details of the sub-harmonic whirling motion of the journal caused by the bearing oil film and limit cycles which cannot be obtained from the linearized model.

A modification of the active bearing with flexible sleeves can be found in reference [7]. To improve attenuation of vibration of a rotor-bearing system, the active bearing was supplied with a hydrodynamic damper. The analysis shows that the stability of the system equilibrium position can be significantly improved by an optimal selection of damper parameters.

The effectiveness of the active bearing with flexible sleeves in the attenuation of vibration by means of the self-tuning adaptive control was studied in reference [8]. Authors concluded that the proposed self-tuning controller was suitable for the forced vibration control of the rotor system by incorporating the active journal bearing. The amplitude of the synchronous vibration due to rotor imbalance can be effectively reduced.

The results summarized above require verification by means of experimental investigation. This paper presents experimental verification of the modelling technique of a multi-bearing rotor system incorporating the active journal bearing with the flexible sleeve studied in references [6, 8].

2. DESCRIPTION OF THE EXPERIMENTAL RIG

Figure 1 shows the schematic diagram of the experimental rig. The rotor 2 is supported upon three bearings. The middle active oil bearing is shown in detail in Figure 2. Similar to a common design of journal bearing, the bearing bush and the main housing are made from different materials and manufactured separately. The bush is made from bearing bronze, and the main housing from steel. Unlike a conventional journal bearing, the bearing bush consists of three separate parts

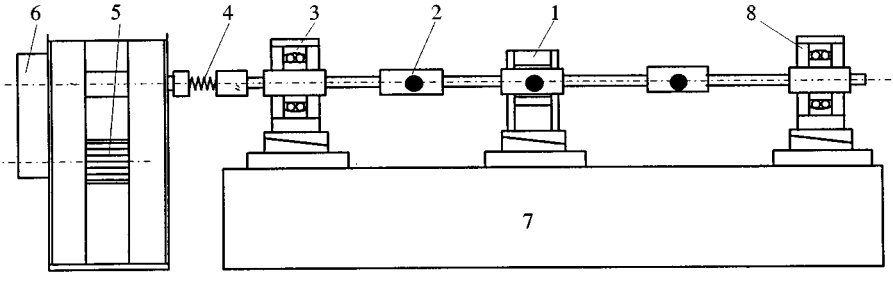

Figure 1. Schematic diagram of the experimental rig: 1-active journal bearing; 2-rotor; 3 and 8-ball bearings; 4-flexible coupling; 5-motor; 6-belt transmission system; 7-foundation; ● nodes of the condensed rotor model.

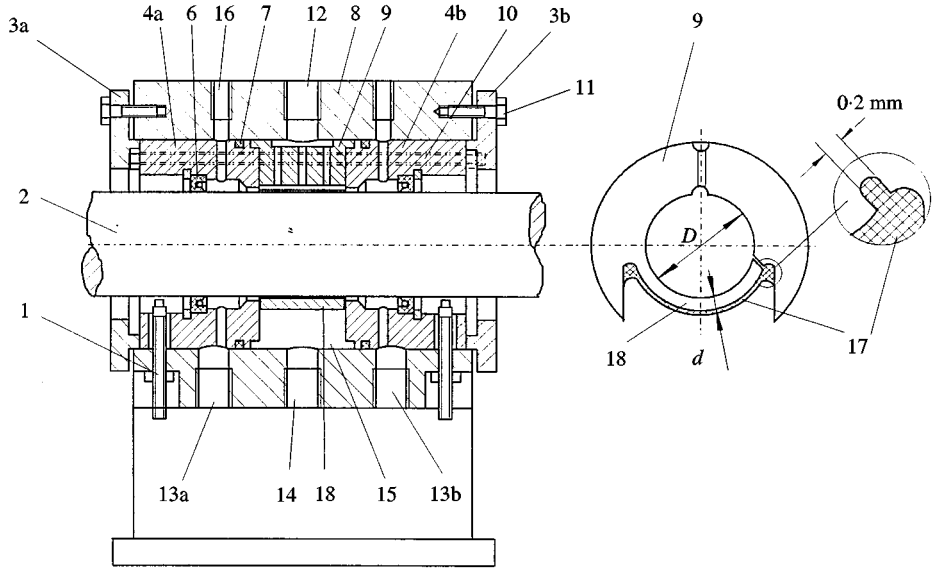

Figure 2. Assembly of the active bearing: 1-eddy current transducer; 2-journal; 3-flanges; 4-bearing bushes; 6-lip-seal; 7-"O" ring seal; 8-housing; 9-bearing bush; 10-bolt; 11-bolt; 12-lubricant inlet; 13-lubricant outlets; 14-chamber pressure input; 15-pressure chamber; 16-air channels; 17-flexible sealant; 18-flexible sleeve.

(parts 9, 4a and b). Part 9, as shown in Figure 2, contains the bearing sleeve (including the flexible sleeve), and the lubricant oil inlet 12. The lubricant oil outlet and oil seals (including the main lip-seal 6 and the "O" ring seal 7) are accommodated in parts 4a and b of the bearing bush. These three parts are assembled together by two bolts 10 before they are put into the main housing. Then this bush assembly is retained in the main housing firmly by flanges 3a, b and bolts 11.

The bush assembly and main housing 8 form the pressure chamber 15, to which the pressure is supplied through the connecting screw socket 14. The gaps at the free end of the flexible sleeve and between the flexible sleeve and the surfaces of parts 4a, b as shown in Figure 2 are sealed by adhesive silicone rubber, which forms a flexible sealant. Therefore, the flexible sleeve can move freely under the chamber pressure, and on the other hand, the pressure in the chamber will not influence the boundary condition of the pressure distribution in the oil film between the journal and the bearing sleeve.

The holes 16 in the lubricant outlet chambers are connected with two valves leading the chambers to the air. A suction pump is connected to the outlet chambers by the two fittings (13a, b) at the bottom of the outlet chambers to drain the lubricant oil collected in the chambers and return it to an oil tank. Therefore, the outlet boundaries of the oil film between the bearing sleeve and the journal are open to the atmosphere, which prevents negative pressure from being developed in the oil film.

Parts 4a and b also form two sleeves, adjacent to the bearing sleeve in part 9. The radial clearance between these sleeves and the journal is twice the bearing clearance

between the sleeve of part 9 and the journal, disregarding the deformation of the flexible sleeve. These two sleeves serve as a back up bearing in case the vibration amplitude of the flexible sleeve is too high, or the flexible sleeve is broken due to fatigue or any other reason.

The flexible sleeve 18 can be considered as a new feature of the proposed active journal bearing. It is activated by the pressure p_c in the chamber 15, which is controlled by valves in the hydraulic system. By adjusting the chamber pressure one can control the deformation of the flexible sleeve. Therefore, the geometry and thickness of the oil film, and subsequently the dynamic properties of the rotor system, can be controlled without stopping the operation of the machine. The chamber pressure can also be changed dynamically by a servo valve. So the active journal bearing can deliver dynamic control forces to the rotor via the oil film to control the forced vibration by either an open-loop means or feedback approaches. Since the rotor is supported upon three bearings (see Figure 1), it is statically indeterminate. It follows that the bearing alignment influences the system dynamic behaviour. To study this influence, the pedestals of these bearings can be shifted. Figure 3 presents the shifting mechanism.

A pair of wedges 2 and the adjustment bolts 3 realize the vertical shifting of the bearing. The upper wedge is fixed with the bearing while the lower wedge can be moved horizontally by the adjustment bolts 3. The inclination of the wedges are 10 : 1 and the thread pitch of the bolts is 1 mm. Therefore, with each turn of the bolts, the bearing is shifted by 0·1 mm. The total shifting range in the vertical direction is 4 mm. The differential bolt 5 produces the horizontal shifting. The coarse thread (with 1·25 mm pitch) of the differential bolt is mounted in the base plate 6, while the fine thread with 1 mm pitch is mounted in the horizontal shift unit

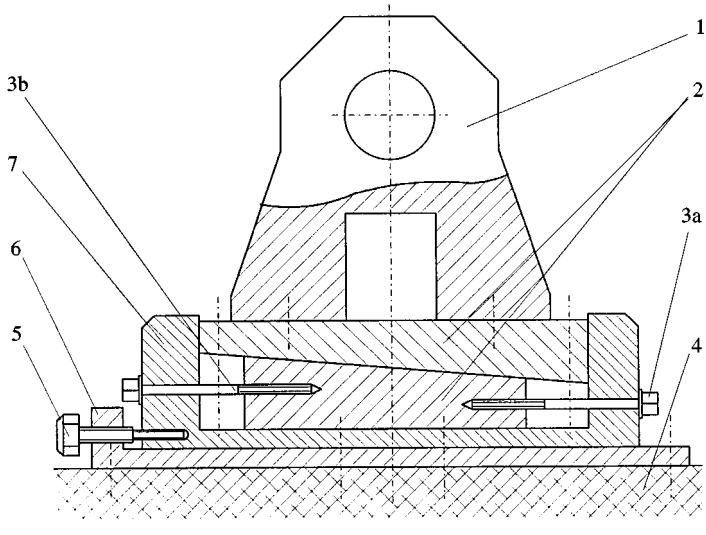

Figure 3. Shifting mechanism of bearing pedestal: 1-bearing; 2-vertical shift wedges; 3-vertical shift adjustment bolts; 4-foundation; 5-differential bolt for horizontal shift adjustment; 6-base plate; 7-horizontal shift unit.

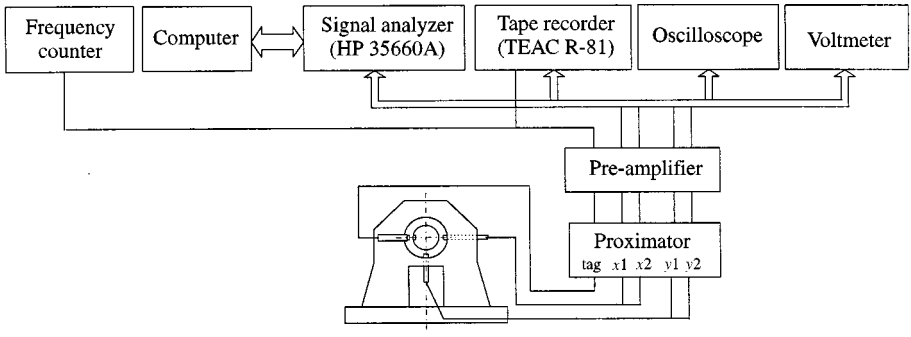

Figure 4. Diagram of the measurement instrumentation.

7. The total shifting range in the horizontal direction is 4 mm. During the shifting operations, two dial gauges with an accuracy of 0·001 mm were used to monitor the shifts of the bearing in both the horizontal and vertical directions.

The shifting mechanisms are mounted on a heavy concrete foundation block, that can be considered rigid in the dynamic analysis.

Figure 4 shows the block diagram of the measurement system. The journal to bearing displacement is measured using Bently Nevada 7200 series 5 mm eddy current displacement transducers with a sensitivity of 8 V/mm. Four transducers are used in the active journal bearing, two for the vertical and two for the horizontal direction. These signals are sent to the signal analyzer for digital analysis. Then, in the digital form, they are transferred to the computer via the GPIB488 parallel interface for further data analysis and processing.

Another eddy current transducer is used to measure the rotating speed of the rotor. The rotor was driven by an AC motor 5 via a belt transmission system 6, and a flexible coupling 4 between the driving system and the rotor 2, as shown in Figure 1. The motor speed controller produces AC current with adjustable frequency in range 1–50 Hz. The nominal speed of the motor was 1400 r.p.m. at the supply frequency of 50 Hz. The speed ratio of the belt transmission system was 71 : 30.

The experimental rig was pre-aligned before the rotor was installed. The pre-alignment provides a reference in the investigation of the effect of the system configuration parameters on the system dynamic behaviour. A laser gun and optical targets were used to pre-align the laboratory installation.

A more detailed description of the test rig can be found in reference [9].

3. THE MATHEMATICAL MODEL OF THE EXPERIMENTAL RIG

The equations of motion of the flexible sleeve can be adopted as follows:

$$\mathbf{M}_s \cdot \ddot{\mathbf{r}}_s + \mathbf{K}_s \cdot \mathbf{r}_s = \mathbf{H}_s + \mathbf{C}_s, \tag{1}$$

where $\mathbf{r}_s$ is vector of the sleeve co-ordinates. $\mathbf{M}_s$ and $\mathbf{K}_s$ stand for the condensed mass and stiffness matrices. $\mathbf{H}_s$ and $\mathbf{C}_s$ represent the hydrodynamic forces due to the

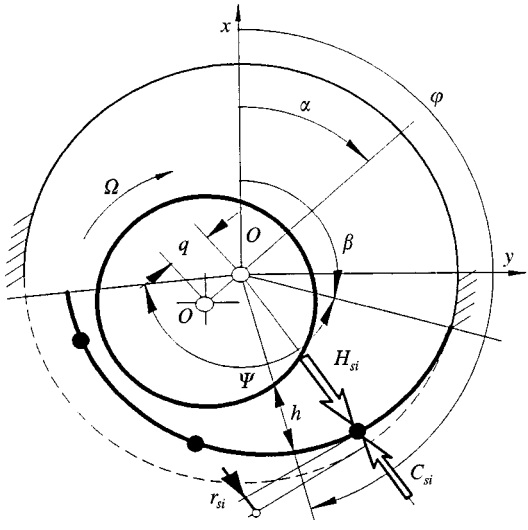

Figure 5. Physical model: - configuration of the active bearing; ● - nodes of the condensed model of the flexible sleeve.

instantaneous oil film pressure p and the chamber pressure p_c respectively (see Figure 5). Division of the flexible sleeve into the final elements as well as the adopted condensation technique are addressed in detail in reference [6].

The Reynolds equation was used to model the pressure distribution p.

$$\frac{1}{R^2}\frac{\partial}{\partial\varphi}\left(\frac{h^3}{\eta}\frac{\partial p}{\partial\varphi}\right)+\frac{\partial}{\partial z}\left(\frac{h^3}{\eta}\frac{\partial p}{\partial z}\right)=6\Omega\frac{\partial h}{\partial\varphi}+12\frac{\partial h}{\partial t}. \tag{2}$$

R, z and φ form the cylindrical system of co-ordinates. The angular speed of the rotor is denoted by Ω, η is the oil viscosity and t stands for time. The thickness of oil film h depends on the instantaneous deformation of the flexible sleeve r_{si} and relative positions q of the journal and the bearing. Therefore, pressure p is a function of these instantaneous displacements, their velocities and the rotating speed of the rotor, i.e., $p = p(\Omega, \mathbf{r}_s, \mathbf{q}, \dot{\mathbf{r}}_s, \dot{\mathbf{q}})$. The integration of equation (2) produces the oil film pressure distribution p. The principle of virtual work applied to the instantaneous oil pressure p results in the hydrodynamic forces $\mathbf{H}_s$ acting on the flexible sleeve. The same principle applied to the chamber pressure p_c yields the force vector $\mathbf{C}_s$.

The equations of motion for the transverse vibration of the rotor can be expressed in the form

$$\mathbf{M}_r\cdot\ddot{\mathbf{q}}+\mathbf{K}_r\cdot\mathbf{q}=\mathbf{H}_r+\mathbf{Q}_r-\mathbf{K}_r\cdot\mathbf{a}+\mathbf{F}_r. \tag{3}$$

$\mathbf{M}_r$ and $\mathbf{K}_r$ are the mass and stiffness matrices of the rotor. $\mathbf{Q}_r$ and $\mathbf{F}_r$ represent the static load and the external excitation forces acting on the rotor due to the residual

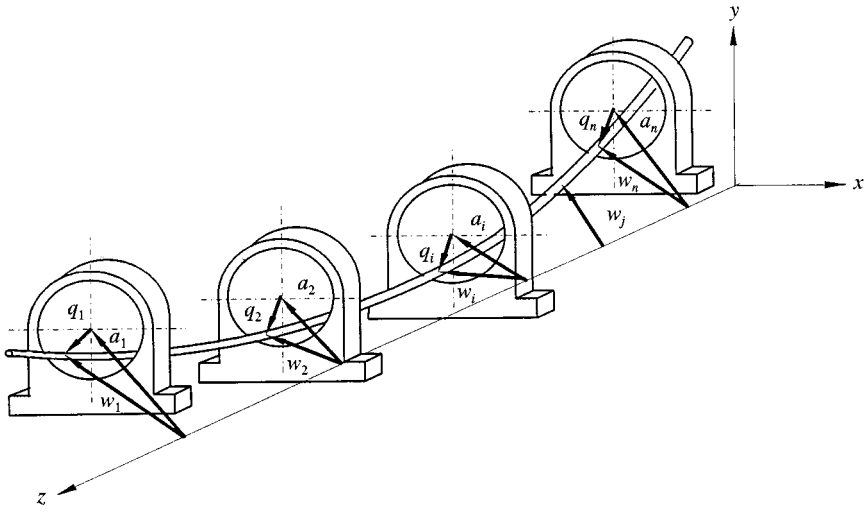

Figure 6. Physical model: -configuration of a multi-bearing-rotor system.

unbalance respectively. $\mathbf{H}_r$ is the vector of hydrodynamic forces caused by the oil film. The configuration of the rotor system (misalignment) is denoted here by **a**, while **q** stands for vector of the relative positions of the bearing and the journal (see Figure 6). Analysis of the gyroscopic effect leads to conclusion that within the operating range of the laboratory installation it influences the natural frequencies by less than 2%. Therefore, the gyroscopic effect was neglected in the presented numerical simulations.

Equations (1) and (3) form a simultaneous set of the non-linear differential equations coupled by the hydrodynamic forces governed by equation (2). These equations were solved by means of numerical methods. The authors used the Runge–Kutta method for the numerical integration of equations (1) and (3), and the finite difference method for solution of equation (2). Details of this mathematical model as well as problems associated with its numerical integration could be found in reference [6].

This mathematical model was solved here for parameters that correspond to the described laboratory installation. The rotor length is equal to 2 m and its weight is 11·24 kg. The active bearing is located 663 mm from the left ball bearing and 1037 mm from the right one (see Figure 1). The other parameters of the test rig are bearing length to diameter ratio $L/D = 0{\cdot}8$; bearing nominal radial clearance $c = 0{\cdot}3$ mm; $\beta = 105^\circ$ and $\Psi = 160^\circ$ (see Figure 5); bearing diameter $D = 50$ mm; thickness of the flexible sleeve $d = 5$ mm; (see Figure 2); lubricant viscosity $\eta = 0{\cdot}04$ Pa s.

The rotor was modelled by the FEM with 26 elements and 104 d.o.f. The final condensed model contains only three rotor nodes (see Figure 1) with only 6 d.o.f. The FEM was also used to model the flexible sleeve. The flexible sleeve was divided evenly into 20 elements with 60 d.o.f. The final condensed model has 3 d.o.f. associated with three nodes shown in Figure 5. It has been found that the final condensed models have eigenvalues and eigenvectors almost identical to the

original FEM models up to the second mode for both the rotor and the flexible sleeve. The accuracy of the third eigenvalue is about 5% for the rotor and 6% for the flexible sleeve. The three eigenvalues of the condensed models are 10·43, 43·04 and 106·38 Hz, respectively, for the rotor, and 490·2, 1754·2 and 6175·8 Hz respectively for the flexible sleeve.

4. RESULTS OF THE NUMERICAL SIMULATION AND THE EXPERIMENTAL VERIFICATION

4.1. STATIC DEFORMATION OF THE FLEXIBLE SLEEVE

The measurement of the static deformation of the flexible sleeve under different chamber pressures was carried out before the journal was inserted into the bearing. The schematic diagram of the measurement is shown in Figure 7(b). A Bently Nevada eddy current transducer (5 mm in diameter) was used to measure the displacement of the flexible sleeve.

Figure 7(a) shows the measured displacement d of the flexible sleeve at the point corresponding to the third node shown in Figure 5. The theoretical displacement was computed from equation (1) for $\mathbf{H}_s = \mathbf{0}$. The measurement data indicate overall higher system stiffness than the theoretical calculation. This is mainly due to the additional stiffness contribution by the flexible sealant that can be considered as an additional stiffness. The result shows a good linearity over the pressure range from 0·025 to 0·125 MPa. When the chamber pressure is very small ($\leqslant$ 0·025 MPa), there is a small dead zone which may be caused by some non-linear mechanisms in the hydraulic system, the flexible sealant and friction. When the chamber pressure is higher than 0·125 MPa, the gradient of the displacement–pressure curve becomes much smaller. The most possible cause of this phenomemon is due to the non-linearity of the flexible sealant which is confined to the narrow gap at the free end of the flexible sleeve. This phenomenon limits the control ability of the active journal bearing.

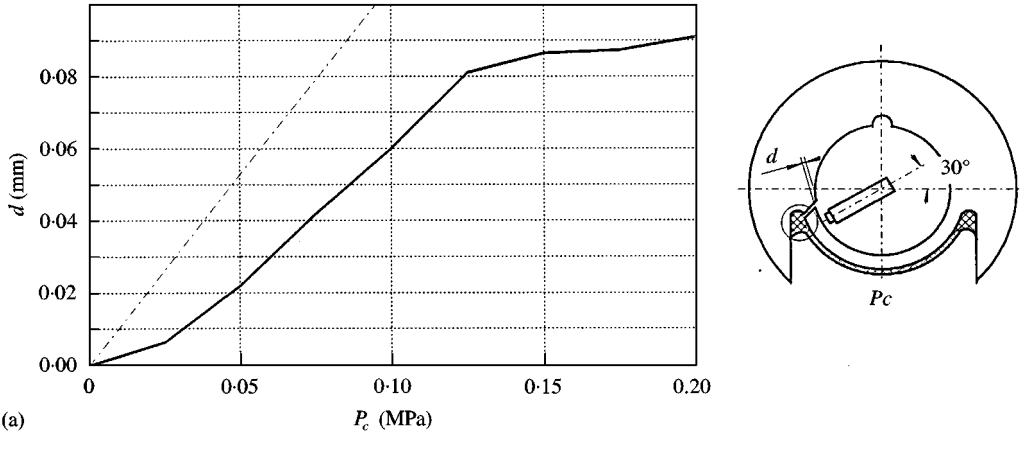

Figure 7. Static deformation of the flexible sleeve: ——, experimental; – · –, theoretical.

4.2 JOURNAL EQUILIBRIUM POSITION VERIFICATIONS

The experimental measurements of the equilibrium position of the journal were carried out under the various system configuration parameters, chamber pressures and shaft rotating speeds. The voltmeter shown in Figure 4 was used to accurately measure the DC component of the signals obtained by the eddy current transducers mounted in the bearing. The oscilloscope was used to monitor the equilibrium position of the journal and to double-check the measurements by the voltmeter. The measured data are then compared with the theoretical calculations obtained by solving the static non-linear equations of the rotor-bearing system (3) [6].

Figure 8 shows the journal equilibrium position obtained by both experimental testing and theoretical calculations for one set of configuration parameters a_x, a_y only ($a_x = 0$ and $a_y = 1$ mm). More experimental data for different sets of configuration parameters could be found in reference [9]. Figure 8(a) shows the case where the rotating speed was fixed but the chamber pressure was changed from 0 to 0·15 MPa with an increment of 0·025 MPa. Figure 8(b) corresponds to the case where the chamber pressure was fixed but the system operating speed was increased from 600 to 2700 r.p.m. with an increment of 300 r.p.m. It can be seen that the

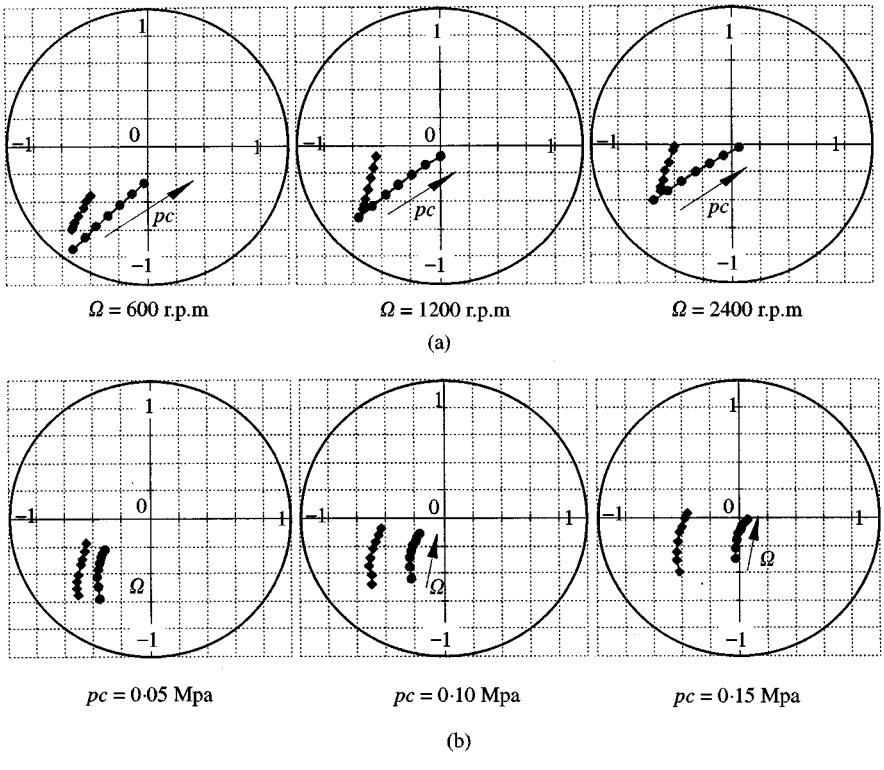

Figure 8. Verification of the equilibrium position: (a) as a function of the chamber pressure p_c; $p_c = 0$–$0{\cdot}15$ MPa; $\Delta p_c = 0{\cdot}025$ MPa; (b) as a function of the angular speed Ω; $\Omega = 600$–2700 r.p.m.; $\Delta\Omega = 300$ r.p.m.; –◆–, results of experimental measurements; –●–, results of computer simulation.

trends of changing of the equilibrium position are consistent between the theoretical and the experimental results. The calculated equilibrium position in the vertical direction agrees quite well with the experimental one. It has been found that the discrepancies in the horizontal direction were mainly caused by the two lip-seals 6 (see Figure 2) used in the test rig which is in close contact with the shaft. The lip-seals exhibit a non-linear hysteresis. Because the hydrodynamic force in the horizontal direction was considerably small with respect to the vertical component, the reaction forces from the lip-seals caused a significant discrepancy between theoretical and experimental results in the horizontal direction.

4.3. SYSTEM RESPONSE VERIFICATION

The forced vibration of the journal due to rotor imbalance was measured using the HP 35660 A Dynamic Signal Analyzer. The theoretical unbalance response of the journal was calculated from the mathematical model obtained by linearization of equation (3) (for details see references [6]).

Figure 9 shows the measured (Figures 9(a) and (b)) and calculated (Figures 9(c) and (d)) journal synchronous response in the horizontal A_x and vertical A_y directions as a function of the rotating speed. The system configuration parameters are $a_x = 0$, $a_y = 1$ mm. The three curves in each graph correspond to the chamber pressure of 0, 0·1 and 0·15 MPa respectively.

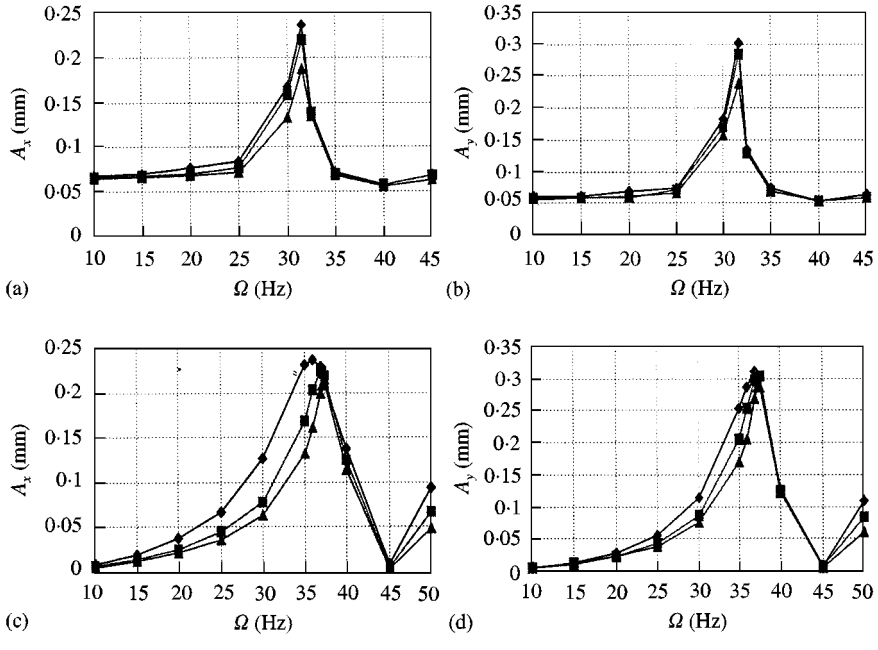

Figure 9. Synchronous response of the journal: (a) and (b) —experimental amplitude; (c) and (d) — theoretical amplitude; A_x — amplitude in the horizontal direction; A_y — amplitude in the vertical direction; –◆–, $p_c = 0{\cdot}00$ MPa; –■–, $p_c = 0{\cdot}10$ MPa; –▲–, $p_c = 0{\cdot}15$ MPa.

The graphs show a reasonable agreement between experimental data and theoretical calculations. Both the experiments and the numerical calculations indicate that a constant chamber pressure has little influence on the critical speed. The first critical speed obtained from experiments is about 32 Hz, and is 37 Hz from theoretical calculations. As a general tendency, with the increase of the chamber pressure, the experimentally measured synchronous vibration decreases. This is consistent with theoretical results.

The discrepancies in the critical speed between experiments and numerical calculations are mainly caused by incomplete modelling of the journal bearing, e.g., due to inaccurate estimation of the oil viscosity. The residual unbalance distribution in the rotor, and an initial bending of the long and thin shaft also affect the agreement between experimental and theoretical results of the forced response of the rotor system.

4.4. STABILITY BOUNDARY VERIFICATIONS

To verify the validity of the mathematical models used for the prediction of the stability boundaries, the chamber pressure thresholds of instability were calculated from the linearized model. Then, the non-linear simulations were carried out to check the results obtained from the linearized model. Finally, the experiments were conducted to verify the results from the numerical calculations. Figure 10 shows the calculated stability boundary based on the linearized model (broken line) as a function of the rotating speed. For this numerical simulation the configuration parameter were chosen to be $a_x = 0$ and $a_y = -2$ mm. This threshold was confirmed by numerical integration of the non-linear equations of motion (3) of the rotor-bearing system. An example of such a computer simulation, carried out for the rotating speed 38 Hz, is shown in Figure 11.

When the chamber pressure is 0·04 MPa (Figure 11(a)), the free vibration of the journal tends to zero and eventually the system reaches a stable equilibrium position. Figure 11(b) presents free vibration of the system for the chamber pressure equal to 0·03 MPa. As one can see, the system tends to a stable equilibrium

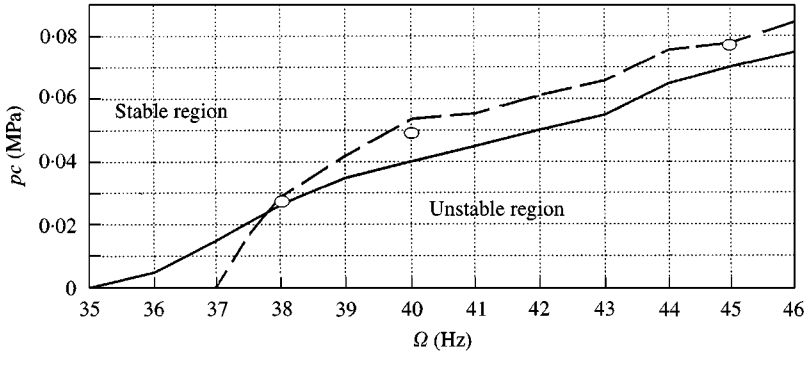

Figure 10. Stability boundaries: ——, experimental data; – –, results of computer simulation (linear approach); results of computer simulation (non-linear approach).

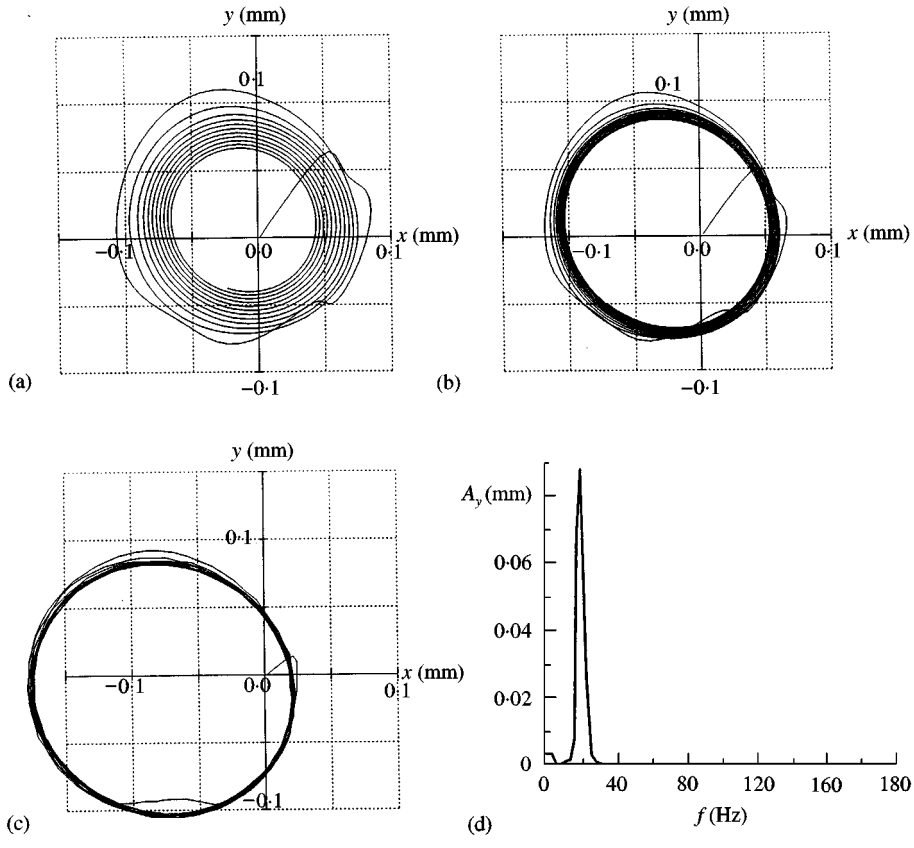

Figure 11. Computer simulation of journal trajectories under different chamber pressures for $\Omega = 38$ Hz; (a) trajectory for $p_c = 0{\cdot}04$ MPa; (b) trajectory for $p_c = 0{\cdot}03$ MPa; (c) trajectory for $p_c = 0{\cdot}02$ MPa; (d) spectrum of the journal response shown in Figure 11(c).

position, but the rate of change of the amplitude of free vibration is much smaller. When the chamber pressure is 0·02 MPa, the journal performs self-excited vibration along a limit cycle shown in Figure 11(c). Therefore, the threshold of stability is between 0·02 and 0·03 MPa. This result is close to the threshold obtained by analysis of the linearized mathematical model (0·029 MPa). Figure 11(d) shows the spectrum of the steady state journal vibration corresponding to the one shown in Figure 11(c). The frequency of the oil whip is 19 Hz, which is equal to half of the rotating speed. Circles, in Figure 10, mark the results of the above computer simulation.

The stability boundary, obtained by the experiments over a range of the rotating speed for the system configuration parameters $a_x = 0$, $a_y = -2$ mm, is shown in Figure 10 by the continuous line. This stability boundary was obtained by means of analysis of journal trajectories. A sample of the recorded journal responses for the rotating speed equal to 38 Hz is presented in Figure 12. Figure 12(a) shows the journal trajectory and its spectrum for the chamber pressure equal to 0·03 MPa. As

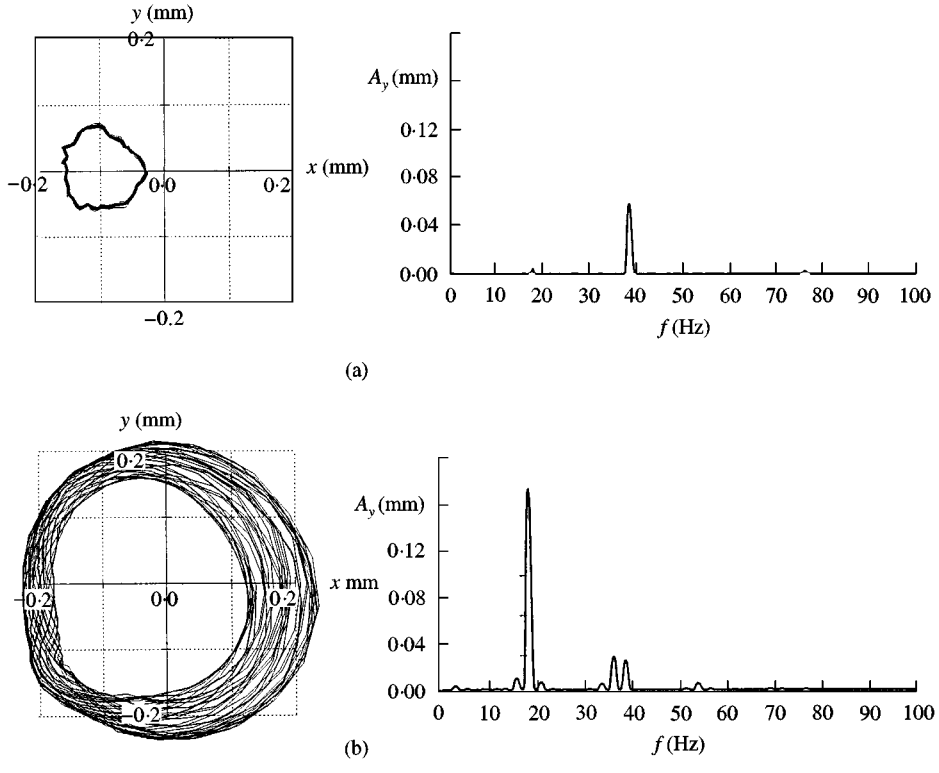

Figure 12. Experimental steady state journal trajectories and the corresponding spectra; (a) in the stable region for $\Omega = 38$ Hz and $p_c = 0{\cdot}03$ MPa; (b) in the unstable region in a stable state for $\Omega = 38$ Hz, $p_c = 0{\cdot}025$ MPa.

one can see, the journal vibrates with a frequency equal to the rotating speed. This vibration is caused by the residual unbalance that is always present in a real system. Therefore, the corresponding equilibrium position is stable. Figure 12(b) presents steady state motion for the chamber pressure equal to 0·025 MPa. The spectrum presented in this figure reveals apart from the forced vibration, large self-excited vibrations (oil whip) of frequency almost equal to a half of the rotating speed. Hence, the equilibrium position is unstable. Therefore, one can conclude that the instability threshold is between 0·025 and 0·03 MPa. The presented data were acquired by the HP 35660A Dynamic Signal Analyzer from the eddy current transducers (see Figure 4).

During experimental investigations, the following two phenomena were observed that contradict to some extent results of the computer simulation.

1. The steady state motion with small component of the self-excited vibration was not observed even if changes in chamber pressure or rotating speed in the vicinity of stability threshold were very small.
2. The stability boundary obtained by a very slow reduction of the chamber pressure was different from the one obtained by increasing the chamber pressure.

The stability boundary shown in Figure 10 was achieved by reducing the chamber pressure (by crossing the boundary from stable to unstable region). The stability boundary, if crossed from the unstable to the stable region, depends on the rate of change of the chamber pressure. The higher the rate of change, the higher is the pressure needed to obtain a stable equilibrium position.

5. CONCLUSIONS

Overall, the numerical calculations based on the mathematical model have shown reasonable agreement with the experimental results both qualitatively and quantitatively. The numerical calculations and the experiments indicate that the stability of the rotor-bearing system is sensitive to the chamber pressure of the active journal bearing. By simply applying an appropriate constant chamber pressure, the system stability can always be improved.

The major cause for discrepancies between numerical and experimental results is the non-linear characteristics of the bearing seals which are not included in the mathematical modelling.

The mathematical model provides useful and good predictions of the system dynamic behaviour, and therefore is very important in the design and analysis of rotor-bearing systems. Both experimental and calculated results have indicated that the active journal bearing provides an effective means of improving the stability of the rotor-bearing system. The stability control approach is simple and reliable which only requires applying an appropriate constant chamber pressure. No sophisticated calculations and feedback systems are required. It is especially significant in industry applications.

Introduction of compressibility and cavitation of the chamber oil into a mathematical model of the active bearing as well as its experimental verification may be considered as a useful extension of the presented work.

REFERENCES

1. G. Schweitzer 1988 *Magnetic Bearings*, *Rotordynamics 2*: *Problems in Turbomachinery* New York: Springer Verlag.
2. A. B. Palazzolo, R. R. Lin, R. M. Alexander, A. F. Kascak and J. Montague 1991 *Transactions of ASME*, *Journal of Vibration and Acoustics* **113**, 167–175. Test and theory for piezoelectric actuator—active vibration control of rotating machinery.
3. J. Althaus and H. Ulbrich 1992 *IMechE 1992*, *C432/045*, 141–148. A fast hydraulic actuator for active vibration control.
4. M. J. Goodwin, J. E. T. Penny and C. J. Hooke 1984 *IMechE*, *C288/84*, 535–541. Variable impedance bearings for turbogenerator rotors.
5. J. Kicinski and P. Materny 1995 *Proceedings of the International Conference on Vibration and Noise*, *Venice*, 120–127. 25–27 April 1995. Non-linear vibrations in multi degree freedom system on the example of turbine 13K215.
6. J. M. Krodkiewski and L. Sun 1998 *Journal of Sound and Vibration* **210**, 215–229. Modelling of multi-bearing rotor system incorporating an active journal bearing.
7. J. M. Krodkiewski, Y. Cen and L. Sun 1997 *International Journal of Rotating Machinery* **3**, 45–52. Improvement of stability of rotor system by introducing a hydrodynamic damper into an active journal bearing.

8. L. Sun, J. M. Krodkiewski and Y. Cen 1988 *Journal of Sound and Vibration* **213**, 1–14. Self-tuning adaptive control of forced vibration in rotor system using an active journal bearing.
9. L. Sun 1996 *Ph.D. Thesis, The University of Melbourne*. Active vibration control of rotor-bearing systems.